Remote Sensing of Environment 311 (2024) 114295

Contents lists available at ScienceDirect

Remote Sensing of Environment

journal homepage: www.elsevier.com/locate/rse

Multitemporal airborne imaging spectrometry and fluorometry reveal contrasting photoprotective responses of trees

Ran Wang [a,*], John A. Gamon [a], Sabrina E. Russo [b,c], Aime Valentin Nishimwe [d], Hugh Ellerman [a], Brian Wardlow [a]

[a] School of Natural Resources, University of Nebraska-Lincoln, Lincoln, NE 68583, USA
[b] School of Biological Sciences, University of Nebraska-Lincoln, Lincoln, NE 68588, USA
[c] Center for Plant Science Innovation, University of Nebraska-Lincoln, Lincoln, NE 68588, USA
[d] Department of Agronomy and Horticulture, University of Nebraska-Lincoln, Lincoln, NE 68583, USA

ARTICLE INFO

Editor Name: Jing M. Chen

Keywords:
Imaging spectrometry
Airborne remote sensing
Solar induced fluorescence (SIF)
Photochemical reflectance index (PRI)
Xanthophyll cycle
Carotenoid pigments
Light use efficiency
Chlorophyll
Functional diversity

ABSTRACT

The Photochemical Reflectance Index (PRI) and solar induced fluorescence (SIF) provide information on plant photosynthetic activity. PRI and SIF are both strongly influenced by irradiance, but uncertainties related to the interpretation of these light responses at large spatial scales remain, partly due to a shortage of suitable data from aircraft or satellite platforms. The goal of this study was to explore interpretations of the PRI- and SIF-light responses of trees owing to species, functional types (evergreen and deciduous) and season. Using airborne hyperspectral and ultraspectral imagery in a North American urban forest, we derived PRI, SIF, and albedo (an indicator of illumination) at the 1-m pixel level. We then quantified crown-level PRI and SIF light responses of ten different tree species at three time points from late-summer to autumnal senescence using hierarchical models. Our results confirmed that both PRI and SIF were strongly influenced by illumination with PRI decreasing and SIF increasing with illumination. Both slope and intercept of the PRI-albedo relationship changed with season, but the pattern varied among species and functional types. SIF values decreased during autumnal senescence for all species, but evergreen species exhibited less seasonal decline in the slope of SIF-albedo relationship compared to deciduous species. The PRI and SIF light responses derived from the airborne imagery offer complementary information on dynamic photosynthesis responses presumably due to varying canopy structure, pigmentation and photoprotection among species and functional types. From airborne platforms, PRI- and SIF-light responses can be used to explore the contrasting physiological responses of individual tree crowns, providing a spatially and temporally explicit view of dynamic plant traits related to photoregulation and a novel view of functional diversity for entire landscapes.

1. Introduction

Remote sensing has long been used to estimate the photosynthetic activity of terrestrial ecosystems. According to the light use efficiency model (LUE; Monteith, 1972, 1977), photosynthetic activity is directly related to the amount of absorbed photosynthetically active radiation (APAR) and the photosynthetic efficiency of the vegetation (ε). Vegetation indices, such as the normalized difference vegetation index (NDVI), the enhanced vegetation index (EVI; Huete et al., 2002), and the near-infrared reflectance of vegetation (NIRv; Badgley et al., 2017) that utilize the red and near infrared bands are able to track slow changes in canopy greenness related to the fraction of PAR absorbed by vegetation (Gamon et al., 1995; Zeng et al., 2022). Along with irradiance (expressed as photosynthetic photon flux density, PPFD), these indices can be used to determine absorbed photosynthetically active radiation (APAR) (Wong et al., 2020), and thus estimate potential gross primary productivity (GPP) over seasonal time scales. The general light use efficiency model form is:

$$\mathrm{GPP} = \int (APAR \times \varepsilon)\, dt \tag{1}$$

The direct estimation of ε, which determines how much of the potential GPP is realized under a given set of conditions, remains challenging because ε varies significantly between individuals, species,

* Corresponding author.
E-mail address: ranwangrs@gmail.com (R. Wang).

https://doi.org/10.1016/j.rse.2024.114295
Received 24 May 2023; Received in revised form 31 May 2024; Accepted 22 June 2024
Available online 28 June 2024

environmental conditions, and ecosystems (Garbulsky et al., 2010). Some LUE models use combinations of lookup tables or meteorological inputs to characterize the dynamic ε term (Running et al., 2004; Yuan et al., 2007). More recent LUE models often attempt to characterize ε by using optical signals (reflectance or fluorescence) of the vegetation to directly indicate real-time adjustment in ε by detecting regulatory changes in energy distribution within the photosynthetic system. Two potential indicators of ε include the Photochemical Reflectance Index (PRI; Garbulsky et al., 2011) and Solar Induced Fluorescence (SIF; Wieneke et al., 2018; Mohammed et al., 2019), because both metrics are sensitive to changes in ε (Wieneke et al., 2018).

Over short time periods, PRI is primarily sensitive to illumination and the epoxidation state of the xanthophyll cycle pigments – violaxanthin, antheraxanthin, and zeaxanthin that regulate heat dissipation of excess light energy, and the quenching of fluorescence via non-photochemical quenching (NPQ), thereby protecting the photosynthetic apparatus (Demmig-Adams et al., 1996; Niyogi et al., 1997; Jahns and Holzwarth, 2012). Under conditions unfavorable for photosynthesis, such as persistent drought or nutrient deficiency or, for evergreens, prolonged winter cold, some plants undergo a sustained downregulation associated with high levels of zeaxanthin (Verhoeven, 2014; Bowling et al., 2018) and altered pool sizes of carotenoid and chlorophyll pigments (Gamon et al., 2016). Zeaxanthin and other carotenoid levels remain high in overwintering evergreen plants during the cold period, presumably maximizing dissipation of light energy to protect leaves during winter (Adams III et al., 2002; Öquist and Huner, 2003). Similarly, pigment pools can vary within canopies according to radiation gradients (Gamon and Berry, 2012; Woodgate et al., 2019). In such cases, PRI variation over long time periods is also influenced by the change in leaf pigment pool sizes (Gamon and Berry, 2012; Garbulsky et al., 2011; Hmimina et al., 2014; Wong and Gamon, 2015; Woodgate et al., 2019). PRI variability caused by short-term ("facultative") and long-term ("constitutive;" Gamon and Berry, 2012) effects has been studied with experiments that measure the change in PRI with increasing illumination (ΔPRI) and the PRI of dark-adapted leaves (PRI_0) (Gamon and Surfus, 1999; Hmimina et al., 2014). To separate the facultative from the constitutive PRI component, a number of variations on the PRI index have been proposed. One of these, the tri-PRI was shown to correct for shifting pigment pool sizes in *Eucalyptus* sp. forests, yielding an index that evaluates the xanthophyll cycle activity (epoxidation state) across canopy position or season (Woodgate et al., 2019). However, to our knowledge, tri-PRI has not yet been evaluated across species at the crown scale with airborne imaging spectrometry. Translating these proximally measured relationships into an image-based remote sensing context has been challenging due to the dearth of scale-appropriate hyperspectral data but has recently been implemented using airborne imaging spectrometry at high spatial resolution (Gamon et al., 2023). In these hyperspectral airborne observations at sub-canopy spatial scales (pixel size ~1m), light intensity and PRI can be estimated at the pixel level, enabling models of the PRI-light responses to be fit for individual tree canopies of different species and different positions in forested landscapes (Gamon et al., 2023). In this method, the intercept and slope estimated from the PRI-light response model have been proposed to correspond to the PRI_0 and ΔPRI from ground studies and reveal substantial variation among individuals, species and locations in their constitutive and facultative PRI responses (Gamon et al., 2023). However, seasonal variation in the PRI-light relationship has not yet been quantified using this light response approach.

Solar induced fluorescence (SIF) has also been used to estimate photosynthesis and detect conditions of stress using remote sensing based on the direct connection between fluorescence signal and photosynthesis (Porcar-Castell et al., 2014). Presumably, the SIF signal is influenced both by APAR and ε, allowing it to faithfully track seasonal changes in photosynthetic activity. However, the degree to which SIF is influenced by APAR *vs.* ε is not always well understood and may vary with spatial and temporal sampling scales (Damm et al., 2022). Furthermore, as with PRI, environmental conditions and vegetation type may also influence SIF responses (Shekhar et al., 2022; Smith et al., 2018; Wieneke et al., 2018). SIF products retrieved from atmospheric chemistry satellites have provided good matches to vegetation photosynthesis integrated over large spatial and temporal scales (Mohammed et al., 2019) and often suggest that APAR is the dominant influence on the SIF signal at these scales (Magney et al., 2019, 2020). Under favorable environmental conditions (suitable temperature, moisture, and nutrient levels), SIF is largely driven by APAR, with an increased ε influence on SIF evident during periods of stress, altering the slope of the APAR-SIF relationship (Zhang et al., 2023). Ground-based SIF measurements (Chang et al., 2020) have been used to try to understand responses of SIF to environmental conditions (Verma et al., 2017; Paul-Limoges et al., 2018), structure and radiation absorption, and photosynthetic downregulation (Zeng et al., 2019; Dechant et al., 2020) to improve its physiological interpretation. These studies show that, as with PRI, SIF is influenced by small-scale variation in illumination and canopy properties, affecting both APAR and ε (Marrs et al., 2020), leading to complex SIF light responses affected by the variation in the within-canopy distribution of PAR (Sun et al., 2023a). Presumably, these effects vary between plant functional types (evergreen versus deciduous), species, and individuals in different conditions, which are largely invisible in satellite-derived SIF measurements due to their coarse spatial and temporal resolutions. If these differences in PRI and SIF light responses can be detected with remote sensing at the sub-canopy level, they can provide a method of detecting differences in species and individual photosynthetic and photoprotective responses, providing a novel view of functional diversity and physiological stress response. Species and functional type differences in PRI and chlorophyll fluorescence have previously been shown in common garden experiments of potted plants (Gamon et al., 1997). Similarly, tree species differences in SIF have been observed from airborne imaging spectrometry (Tagliabue et al., 2019). However, to our knowledge, the relationships between concurrent PRI and SIF-light responses across species have not previously been evaluated using airborne spectrometry.

In this study, we collected simultaneous airborne measurements of PRI and SIF at the ~1-m pixel level for different tree species in an urban temperate forest setting on three dates spanning the transition from the late growing season to early autumnal senescence using the Nebraska Earth Observatory (NEO), an airborne platform outfitted with imaging spectrometer and imaging fluorometer (Wang et al., 2022). By considering spatial patterns of illumination in a single airborne image, our goal was to test the hypothesis that PRI and SIF, particularly when expressed in response to light intensity, can provide complementary information about variation in photosynthetic activity among tree species and functional types through this seasonal transition. Using multitemporal airborne data from two instruments, we predicted that (1) PRI and SIF would exhibit opposite responses to light intensity on each sampling date, with PRI decreasing with irradiance due to increasing energy dissipation and SIF increasing with irradiance due to increasing APAR in the absence of significant stress. (2) PRI and SIF light responses would vary in particular ways (further explained in Fig. 2 in Methods) among the three sampling dates as autumn senescence progressed; and (3) different species and functional types (evergreen vs. deciduous) would exhibit contrasting PRI and SIF light responses due to their different seasonal photosynthetic responses. We aim to provide an initial evaluation of how PRI- and SIF-light responses might enable detection of functional differences in dynamic optical traits related to photosynthesis as represented in the LUE model among species, functional types, and seasons. This approach also provided a preliminary test of the idea that combined reflectance and fluorescence analyses can provide complementary information on photosynthetic function, which is a central theme of the planned Fluorescence Explorer (FLEX) mission (Drusch et al., 2017).

2. Methods

2.1. Airborne data collection and processing

Airborne data for our urban forest study site in the East Campus area at the University of Nebraska-Lincoln (Latitude: 40.83° N, Longitude: 96.67° W; Fig. 1) were collected near solar noon on three days spanning late summer to early fall in 2018 (at 1:16 pm on August 02, 11:18 am on September 17 and 12:52 pm on October 16) using the Nebraska Earth Observatory (NEO). All the images were collected under clear sky to minimize cloud effects. NEO includes an imaging fluorometer (AISA Ibis, Specim, Oulu, Finland) and an imaging spectrometer (AISA Kestrel, Specim, Oulu, Finland) mounted on a fixed-wing piloted plane (Saratoga, Piper Aircraft, Florida, USA). The Ibis imaging fluorometer covers 670 – 780 nm with 0.245 nm spectral resolution (full width at half maximum, FWHM) and the Kestrel imaging spectrometer collects data with 2.4 nm spectral resolution (FWHM) from 400 to 1000 nm. Images were collected from an altitude of 1750 m above the ground level and the instantaneous field of view (IFOV) describing the ground pixels at approximately 1 m. Airborne imagery collected by both sensors were calibrated using lab-measured calibration coefficients to convert to at-sensor radiance ($Wm^{-2}sr^{-1}nm^{-1}$).

To obtain surface reflectance (Kestrel) and radiance (Ibis) from the airborne data, we applied atmospheric correction using the MODTRAN 5 radiative transfer model (Berk et al., 2008). We used the 'mid-latitude summer' atmospheric profile and 'urban' aerosol extinction model to drive the MODTRAN model. The aerosol optical thickness (AOT) at 550 nm was estimated using a modified dense dark vegetation method (Kaufman et al., 1997; Liu et al., 2019). The columnar water vapor (CWV) was retrieved using the 940 nm water absorption band (Carrère and Conel, 1993). The surface reflectance and radiance were then calculated based on the four-stream radiative transfer theory (Verhoef and Bach, 2003). The 0.1 cm^{-1} band model was used in MODTRAN 5 outputs and were further resampled to the Kestrel and Ibis spectral resolution at each band based on Gaussian response functions. Further details of the NEO airborne data processing procedures have been previously documented (Wang et al., 2021, 2022).

The spectral fitting method (SFM; Cogliati et al., 2015) was applied to the atmospherically corrected Ibis data to calculate airborne SIF at the O_2A band (760 nm), considering the higher SIF retrieval accuracy derived from this airborne platform at the O_2A band than the O_2B band (Wang et al., 2022). We calculated PRI using the surface reflectance data collected by the Kestrel imaging spectrometer as

$$PRI = \frac{\rho_{531} - \rho_{570}}{\rho_{531} + \rho_{570}} \quad (2)$$

where ρ_{531} and ρ_{570} indicate the surface reflectance values at 531 nm and 570 nm, respectively.

To help evaluate our interpretation of the PRI light response (details below), we also calculated tri-PRI (TVI; Woodgate et al., 2019), which is intended to isolate the xanthophyll cycle response (facultative PRI response) from the pigment pool size effects (constitutive response). The details and results of this tri-PRI analysis are presented in the Supplemental section.

2.2. Extraction of tree crowns

We used a ground inventory provided by the University of Nebraska-Lincoln Landscape Services to identify 966 trees belonging to 10 species (5 evergreen and 5 deciduous species; Table 1 and Fig. 1) from the

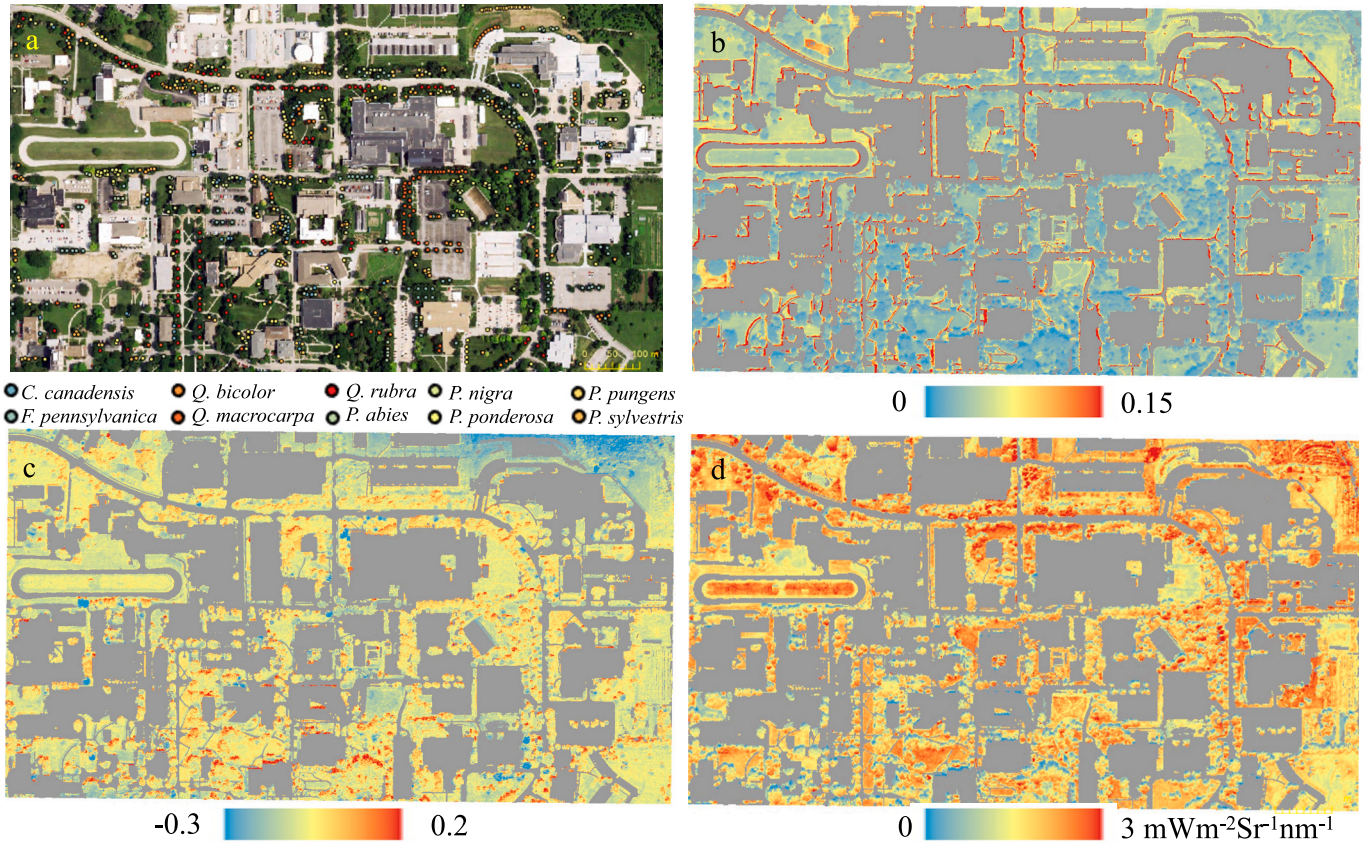

Fig. 1. True color composite (a), PAR albedo (b), PRI (c), and SIF (d) images of the University of Nebraska-Lincoln East Campus area. In panel a, a high resolution (pixel size = 0.6 m) true color aerial image (USDA, 2018) was used to show the locations of trees used in this study (Table 1). In panels b-d, impervious surfaces were shown in grey. NEO images (b,c,d) were collected on August 2, 2018. Tree species data (indicated by colored dots in panel a) were provided by the University of Nebraska-Lincoln Landscape Services.

Table 1
Sampled tree species, functional type, and number of tree crowns of each species

Functional Type	Common Name	Scientific name (family)	No. tree crowns
Deciduous	Eastern redbud	*Cercis canadensis* L. (Fabaceae)	86
Deciduous	Green ash	*Fraxinus pennsylvanica* Marsh. (Oleaceae)	103
Deciduous	White oak	*Quercus bicolor* Willd. (Fagaceae)	97
Deciduous	Bur oak	*Quercus macrocarpa* Michx. (Fagaceae)	95
Deciduous	Red oak	*Quercus rubra* L. (Fagaceae)	101
Evergreen	Norway spruce	*Picea abies* (L.) Karst. (Pinaceae)	83
Evergreen	Blue spruce	*Picea pungens* Engelm (Pinaceae)	87
Evergreen	Black pine	*Pinus nigra* Arnold (Pinaceae)	115
Evergreen	Ponderosa pine	*Pinus ponderosa* Lawson & C. Lawson (Pinaceae)	93
Evergreen	Scotch pine	*Pinus sylvestris* L. (Pinaceae)	106

airborne imagery. Tree crowns were manually identified using GIS software (ArcGIS 10.8, ESRI) and then were used to extract data from each image (6 datasets in total, 3 from Kestrel and 3 from Ibis). The georeferencing error of airborne images was within 2 pixels. To avoid possible edge effects, we removed small tree crowns (number of pixels < 10) from the analysis.

2.3. Hierarchical modeling of the PRI- and SIF- albedo relationship

In order to account for the inherent lack of independence and nesting of pixels within tree crowns, we applied a hierarchical modeling approach to analyze the relationship between airborne products (SIF and PRI) and albedo, following methods decribed by Gamon et al. (2023). We calculated the albedo of tree canopies using data collected by both the imaging spectrometer (Kestrel) and imaging fluorometer (Ibis) to estimate irradiance at pixel level (Gamon et al., 2023). As the sensors had slightly different ground resolutions (IFOV) and pixel locations, we did not match the images on a per-pixel basis, which would have required spatial interpolation and modification of the spectral responses. For the Kestrel data, Photosynthetically Active Radiation (PAR) albedo was calculated as the ratio between reflected energy and total incoming radiation at the 400 – 700 nm spectral range. For the Ibis data, due to the much more limited spectral range of this instrument relative to the Kestrel, we used the albedo at the red bands (670 – 690 nm), which was linearly correlated ($R^2 = 0.93$) to PAR albedo (Figure S1 in the supplemental materials).

We fit hierarchical models to the PRI- and SIF-albedo relationships by setting species as the fixed effect and tree crown as the random effect:

$$PRI_{ij} \text{ or } SIF_{ij} = \beta_0 + \beta_1 \times albedo_{ij} + \varepsilon_{ij}$$

$$\beta_0 = \gamma_{00} + \gamma_{01} \times Species_{ij} + \mu_{0j}$$

$$\beta_1 = \gamma_{10} + \gamma_{11} \times Species_{ij} + \mu_{1j}$$

$$\left(\mu_{0j}, \mu_{1j}\right) \sim N\left(0, \begin{bmatrix} \tau_{00}^2 & \rho\tau_{00}\tau_{11} \\ \rho\tau_{00}\tau_{11} & \tau_{11}^2 \end{bmatrix}\right)$$

$$\varepsilon_{ij} \sim N\left(0, \sigma^2\right) \quad (3)$$

where PRI_{ij} or SIF_{ij} indicates the PRI or SIF value of the ith pixel in the jth tree canopy. This model assumed fixed effect variation (γ_{00}, γ_{01}, and γ_{10}, γ_{11}) of the intercept (β_0) and slope (β_1) by species, as well as random effect variation (μ_{0j} *and* μ_{1j}) of the intercept and slope among tree canopies within species.

We used *pseudo-R^2* statistics to compare the amount of variation due to species (fixed effects) versus individual tree canopies (random effects). The marginal *pseudo-R^2* (R^2M) represents the proportion of variance in the response variable (PRI or SIF) explained by the fixed effect model alone, and the conditional *pseudo-R^2* (R^2C) represents the proportion explained by both the fixed and random effects models (Nakagawa and Schielzeth, 2013). The multilevel model was implemented using the *lmer* function in the LME4 package (Bates et al., 2015) and the *pseudo-R^2* statistics were calculated using the MuMln package (Barton, 2009) in R statistical software (R Core Development Team, 2019). Fitted relationships with 95% confidence intervals were plotted using the GGEFFECTS R package (Lüdecke, 2018). To test if the slope and intercept of the PRI- or SIF- albedo relationships differed between pairs of species, we used pair-wise comparisons and adjusted *P*-values for the number of comparisons performed based on the false discovery rate (FDR) using the Benjamini-Hochberg procedure (Benjamini and Hochberg, 1995). Statistical significance was assessed at $\alpha = 0.05$.

Physiological interpretation of the parameters of the PRI- and SIF-albedo relationship

We hypothesized that the PRI and SIF would show coherent light responses derived from airborne data corresponding to the contrasting photosynthetic and photoprotective responses due to pigment dynamics expected for different species over the summer-fall period (Fig. 2). In this physiological interpretation, the intercept in the PRI light response (PRI-albedo relationship) indicates the constitutive PRI response, corresponding to the relative changes in the chlorophyll:carotenoid pool sizes, which generally declines with senescence of deciduous foliage (Wong et al., 2020, 2022) or with late season transitions to winter downregulation in evergreen trees (Wong and Gamon, 2015; Gamon et al., 2016). The slope in the PRI-albedo relationship indicates the facultative response of PRI, corresponding to changes in the xanthophyll cycle pigments to illumination. A more detailed explanation of this expected PRI light response using airborne imaging spectrometry has been described in (Gamon et al., 2023) and is derived from a history of leaf-level and canopy-level experimental observations of PRI light responses (Gamon and Surfus, 1999; Gamon and Berry, 2012; Hmimina et al., 2014; Magney et al., 2016). In this study, we used a space-for-time substitution and assumed that the slope of the PRI light response obtained from images of whole-canopies would be analogous to the slope

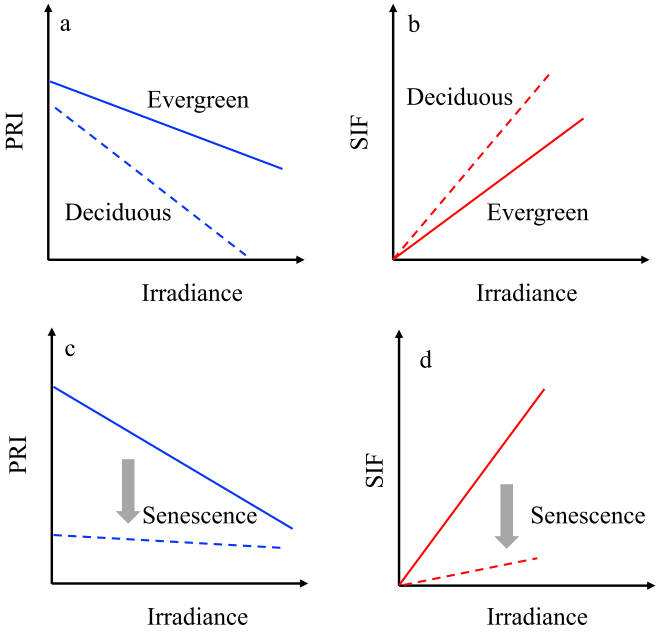

Fig. 2. Hypothetical PRI and SIF light responses between functional types and at different seasons (decreasing photosynthesis, decreasing SIF, and decreasing xanthophyll cycle activity during senescence). In this study, irradiance was estimated using albedo for each pixel derived directly from the airborne imagery.

of the PRI light response reported at the leaf level. This assumption is supported by additional studies (Gamon and Qiu, 1999; Gamon et al., 2005) that have indicated that PRI responds similarly to illumination at leaf and canopy scales for closed canopies, as would be the case in airborne analyses of dense individual crowns. The slope of the SIF light response curve (SIF-albedo relationship) indicates the light use efficiency (Zhang et al., 2023), whereas the intercept in the SIF-albedo relationship should always be close to zero, because SIF is driven by absorbed radiation and thus should equal zero under dark conditions. In summary, PRI is expected to track light use efficiency due to both constitutive and facultative responses, which represent slightly different mechanisms occurring on different time scales. By contrast, SIF is expected to respond both to APAR and efficiency (higher APAR leads to larger SIF values, and higher efficiency leads to a steeper slope in the SIF-light response).

Under conditions favorable for photosynthesis, we expect PRI to decline and SIF to increase with irradiance (Fig. 2 a&b). On each sampling date, differences in the PRI and SIF light response curves between species and functional types presumably reveal variation in the underlying leaf photosynthetic and photoprotective responses. During autumn senescence of the deciduous species, we expected that the PRI light response slope would become shallower with loss of xanthophyll cycle pigment function (affecting the slope), and with the more rapid decline of chlorophyll pigments relative to carotenoid pigments (affecting the intercept; Fig. 2c). We expected that the slope of the SIF light response would become shallow (less responsive to irradiance), typically indicating a decline in light use efficiency during senescence. Since we did not directly measure APAR, the decline in the slope of the SIF light response could also be confounded by chlorophyll losses in the fall. These canopy-scale hypotheses, illustrated in Fig. 2, were tested using the light-response approach applied to airborne data as described above. In addition to these canopy-level tests, we independently tested these variations of PRI and SIF light responses in a small sample of individual leaves collected in late fall and exhibiting different stages of

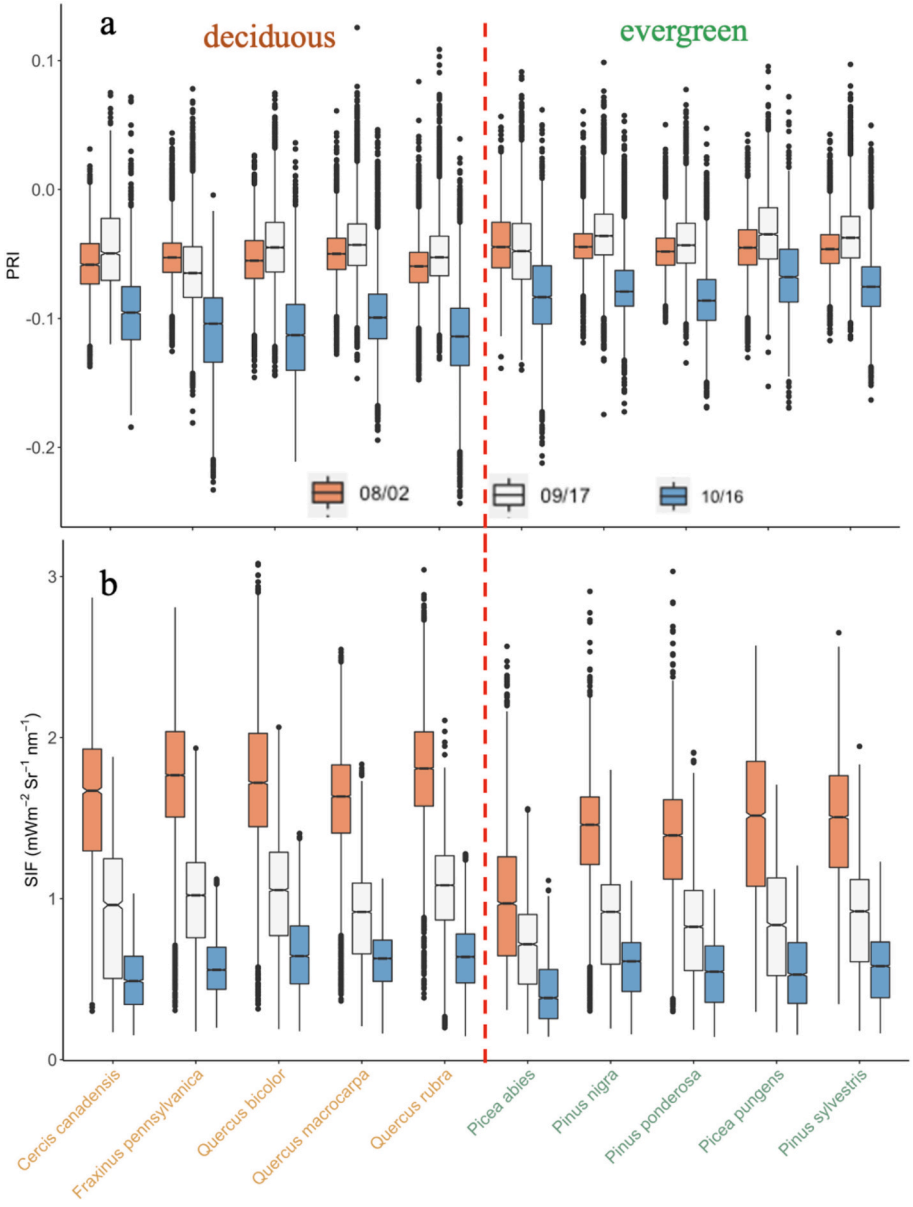

Fig. 3. Canopy average PRI and SIF values of different species collected on the three sampling dates. The line in the middle of each box indicates the median value. The lower and upper hinges correspond to the first and third quartiles (the 25th and 75th percentiles) and data beyond 1.5 times the distance between the first and third quartiles from the lower and upper hinges are plotted as individual points. The medians are roughly significantly different at a 95% confidence level, if the notches do not overlap (McGill et al., 1978). A red dashed line separates the deciduous and evergreen species.

senescence to confirm the general pattern of leaf-level light responses (Figure S2 in the supplemental materials). The resulting leaf-level patterns qualitatively agreed with the responses predicted for tree canopies (Fig. 2). To illustrate the additional information provided in the light response approach, we also calculated canopy average PRI and SIF values for each individual tree, representing the values that would be obtained with sensors having coarser spatial resolution.

3. Results

When expressed as average canopy responses, canopy reflectance spectra exhibited a steady increase in the visible region and a decline in the near-infrared region towards fall, indicative of pigment loss and leaf senescence over the study period (Figure S3 in the supplemental materials). Canopy average PRI changed little from August to September, then dropped between September and October (Fig. 3a), and this drop was most noticeable in the deciduous species that were undergoing leaf senescence. By contrast, canopy average SIF values decreased steadily from August to October for all species, likely indicating a decline in photosynthetic rate from summer to fall (Fig. 3b). For PRI, the largest change was from September to October, whereas for SIF the largest change was from August to September, suggesting that SIF and PRI provide slightly different information regarding seasonally changing photosynthetic activity. The patterns of seasonal change in PRI and SIF varied between evergreen and deciduous species (Fig. 3). Evergreen species tended to have slightly larger average PRI values than deciduous species on all three sampling dates, and this pattern was most obvious in the October data (Fig. 3a), when leaves of deciduous species had begun senescence. Evergreen species also tended to show smaller SIF values than deciduous species in August and September, but these differences in SIF between evergreen and deciduous species diminished by October (Fig. 3b). Overall, deciduous species exhibited higher average SIF, but smaller average PRI values than evergreen species, and the differences in SIF values between these two functional types decreased, while differences in PRI values increased during autumnal senescence. These canopy average PRI and SIF values, contrasted with the metrics based on light responses, illustrating additional information in the light response approach.

When expressed as a light response by plotting PRI and SIF as a function of albedo instead of as canopy average values, a more nuanced picture emerged (Fig. 4). As expected, across all tree canopy pixels, PRI declined and SIF increased with albedo (Fig. 4), a measure of relative canopy illumination. Variations in PRI and SIF were primarily explained by albedo, indicating a strong light response in both cases, but these light responses also differed with species, expressed as improved hierarchical model fits when adding the interaction term between albedo and species (Table 2 and Fig. 5). Besides the species differences in the PRI or SIF – albedo relationships (R^2M), substantial within-species and among-individual variation occurred (R^2C, Table 2), indicating that species and individual canopy variation added to the overall variation in PRI and SIF light responses, and demonstrating an ability of these light responses to detect functional differences between individual tree crowns and species.

Examination of the intercepts and slopes from the PRI-albedo relationship allowed us to explore the constitutive versus facultative effects (*sensu.* Gamon and Berry, 2012) on the PRI-albedo relationships among

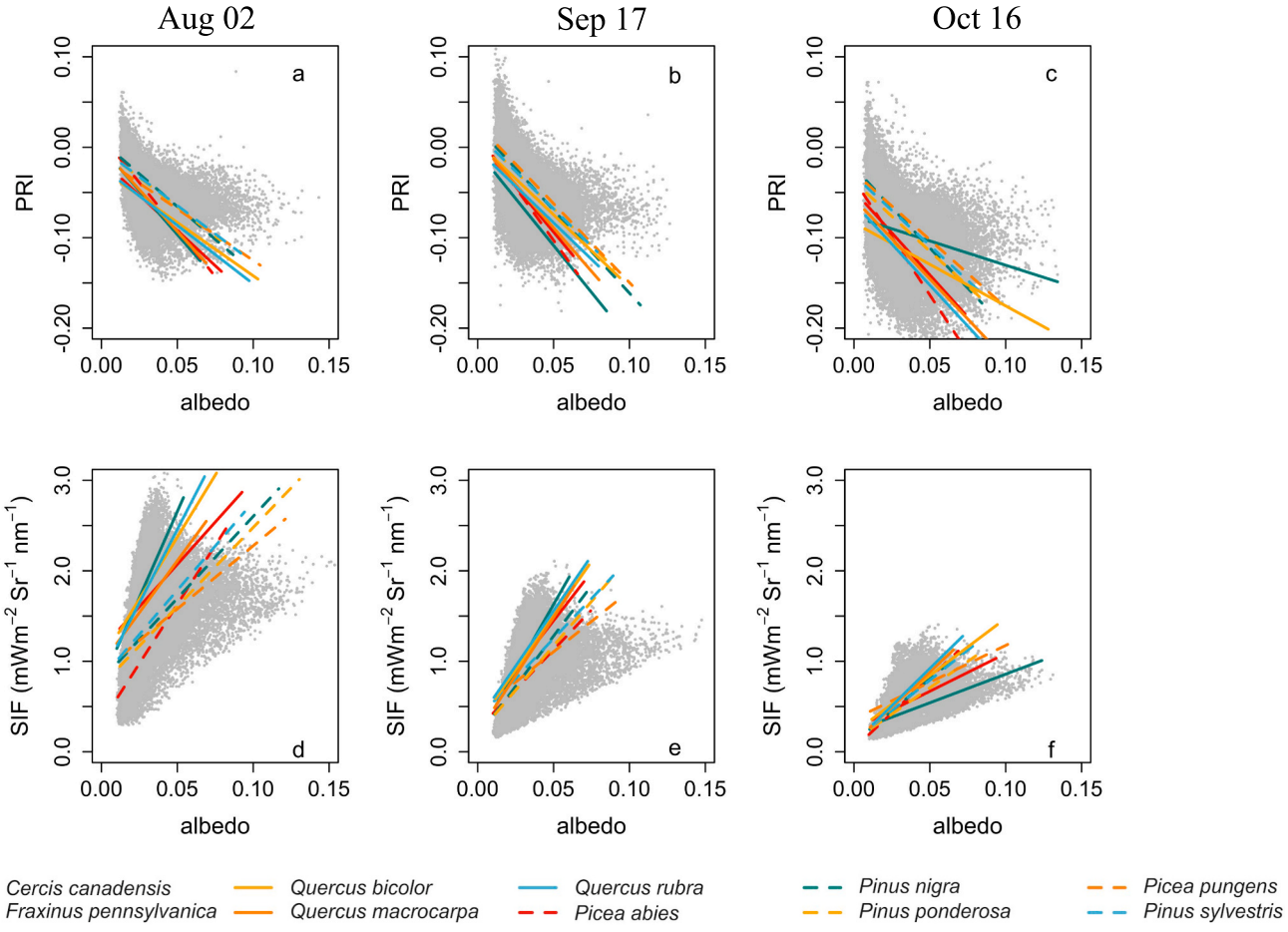

Fig. 4. PRI (a, b, c) and SIF (d, e, f) against albedo (a proxy for irradiance) on the three sampling dates (a & d: August 02; b & e: September 17; c & f: October 16), with colored lines indicating fitted hierarchical models for different species, and dots representing individual pixel values. Fitted intercepts and slopes for each species are shown in Fig. 5. The number of tree crowns of each species was summarized in Table 1.

Table 2
Hierarchical model analysis of the relationships between the photochemical reflectance index (PRI) or solar induced fluorescence (SIF) and albedo, species identity, and individual tree crowns. P-value < 0.001 for all three terms (albedo, species, and interaction) in an ANOVA test of each model. The numbers in parentheses indicate the sampling date (MM/DD). The marginal pseudo-R^2 (R^2m) represents the proportion of the variance explained by the fixed effects model alone, and the conditional pseudo-R^2 (R^2c) represents the proportion explained by the fixed and random effects models together.

Variable (Date, MM/DD)	*F*-value			R^2m	R^2c
	albedo	species	species × albedo		
PRI (08/02)	1266.76	8.39	6.25	0.34	0.89
PRI (09/17)	1833.8	5.17	2.99	0.43	0.82
PRI (10/16)	1044.46	22.22	12.48	0.28	0.89
SIF (08/02)	830.06	5.66	8.87	0.36	0.9
SIF (09/17)	1367.1	2.96	6.4	0.48	0.92
SIF (10/16)	1623.28	5.89	12.91	0.4	0.93

species and over time (Fig. 5). Intercepts in the PRI-albedo relationships (indicative of chlorophyll:carotenoid pool sizes) increased slightly from August to September then decreased from September to October. Slopes in the PRI-albedo relationships (indicative of xanthophyll cycle responses to irradiance) decreased markedly from August to September then increased slightly from September to October. These responses suggest separate effects on pigment pool sizes (constitutive effects affecting intercepts) and xanthophyll cycle activity (facultative effects affecting slopes). Evergreen species showed higher intercepts in the PRI-albedo relationship than deciduous species, whereas deciduous species had overall steeper slopes in the PRI-albedo relationship than evergreen species (Fig. 5a), suggesting a different partitioning of facultative and constitutive effects between vegetation types.

Deciduous species exhibited larger variations in the slopes of SIF-albedo relationships than evergreen species in August and September (Figs. 5d and S4 in the supplemental materials). In October, evergreen species had larger slopes in the SIF-albedo relationship than deciduous species. In August, larger variation occurred in slopes of the SIF responses than those of PRI, but less variation was found in slopes of the SIF light responses than those of PRI in October. Presumably, the slopes from the SIF-albedo relationship provided information about how the photosynthetic light use efficiency varied among species and over time but could also be further influenced by the loss of pigments or altered canopy structure with the onset of leaf senescence.

Pairwise comparisons of differences in the intercept and slope between species enabled us to explore contrasts in species and functional type PRI and SIF light responses at different times during the transition from summer to autumn. Several pairs of species differed in slopes, intercepts, or both ($p < 0.05$; orange squares in Fig. 6), suggesting interspecific variation in photoprotection. For the PRI-albedo relationship, greater among-species differences occurred in October than August and September, especially between deciduous and evergreen functional groups. For the SIF-albedo relationship, as expected, among-species difference occurred mainly in the slopes but not intercepts, except for *Picea abies* in August and *Picea abies* and *Pinus ponderosa* in October. The light responses of *Fraxinus pennsylvanica* (green ash) stood out from the rest of the species, and this was clear across the PRI and SIF light responses. This species showed particularly abrupt changes in the slopes of PRI and SIF between September and October (Fig. 5), reflecting a more rapid fall senescence relative to the other deciduous species. We also

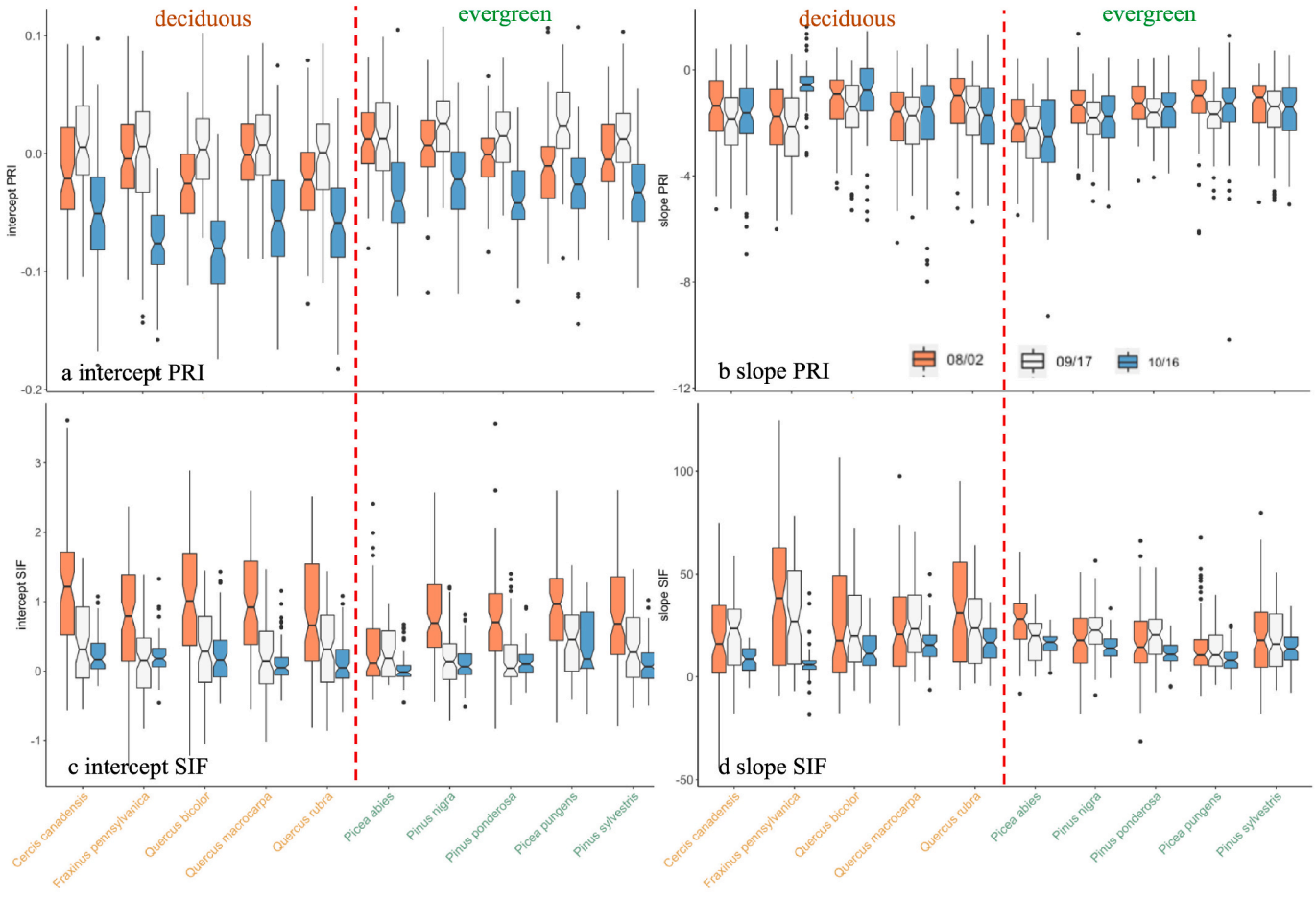

Fig. 5. Intercepts (a & c) and slopes (b & d) of the fitted PRI-albedo and SIF-albedo relationships. The red dashed lines separate the deciduous and evergreen species.

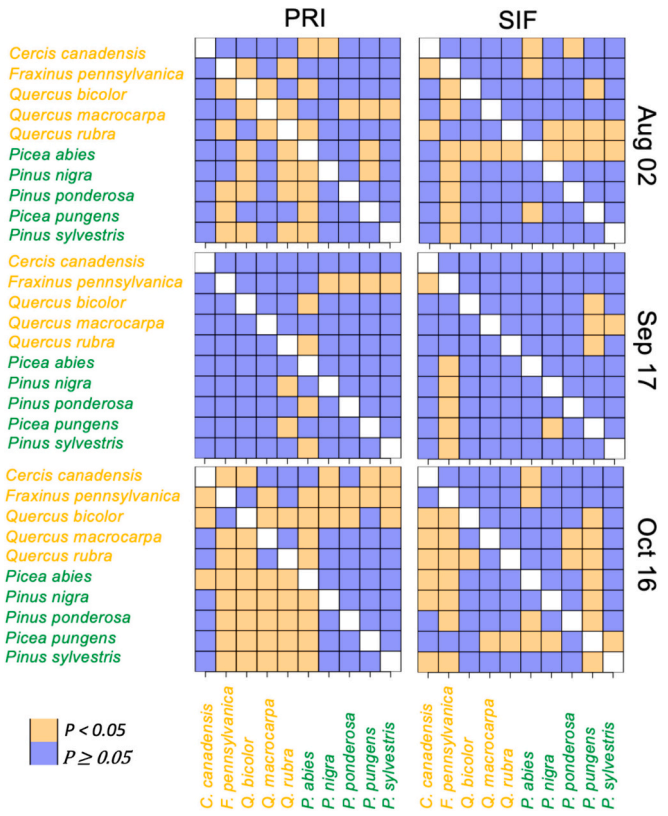

Fig. 6. *P*-value matrices showing pair-wise comparisons of intercept and slope of the PRI – albedo (left column) and SIF – albedo (right column) relationship tests between species. *P*-values were adjusted based on the DFR using the Benjamini-Hochberg procedure (Benjamini and Hochberg, 1995). Orange squares indicate significant difference in intercept (upper triangle) and/or slope (lower triangle) between species.

noted a marked change in the PRI intercept, and a parallel increase in the visible reflectance for this species (Fig. 5 & Fig. S3) between September and October, consistent with advanced leaf senescence.

Direct comparison between *Fraxinus pennsylvanica* (a deciduous species that showed earlier senescence than the rest of the species) and *Picea abies* (an evergreen species that retained its foliage) illustrated the differences in PRI and SIF light responses between the two extreme cases representing two functional types (Fig. 7). Small changes in intercepts in PRI light responses from August to September and large changes in intercepts in PRI light responses from September to October were found for both species. Slopes in SIF light responses decreased over the season for both species, but *Fraxinus pennsylvanica* had a larger change from September to October, while *Picea abies* had a larger change from August to September. Particularly noticeable was the large change in both PRI and SIF light responses with the beginning of fall senescence in October. *Fraxinus pennsylvanica* (green ash) exhibited much shallower slopes in October than in August and September due to early leaf pigment loss during fall senescence. On the other hand, *Picea abies* (Norway spruce) showed a steeper PRI light response and shallower SIF light response, suggesting greater photosynthetic downregulation (lower ε), in October than in August and September, consistent with a fall decline in photosynthesis as colder temperatures emerge.

4. Discussion

The ability to predict changes in photosynthetic activity of individuals and species over large extents and through time is important for quantifying vegetation responses to environmental stressors, including extremes in temperature, nutrients, water status, pests, and disease. PRI and SIF are two metrics often used for this purpose, but their strong light-dependence complicates interpretations with respect to stress-related changes in photosynthetic activity and efficiency. The tendency for PRI and SIF to be affected by both physiological and structural factors further complicates the mechanistic interpretation of these signals. Here, we demonstrate that accounting for illumination (using albedo as an irradiance proxy) revealed key differences in PRI and SIF light responses among tree crowns, species and functional types during the summer-fall transition. Modeling and analyzing the fitted parameters (slope and intercept) of the PRI and SIF light response relationships provided additional insights into the functional differences in the PRI and SIF responses that were not readily apparent in canopy average values, and demonstrate the utility of airborne imagery for resolving contrasting variable light responses of individual tree canopies.

4.1. PRI and SIF light responses over the season

The PRI light response enabled us to distinguish the constitutive (intercept in the PRI-albedo relationship) and facultative (slope in the PRI-albedo relationship) effects at the canopy level, which have been previously studied with proximal spectroscopy at the leaf scale (e.g., Gamon and Berry, 2012) and have recently been demonstrated at the canopy scale (Gamon et al., 2023). Different intercepts suggest variation in the composition of photosynthetic chlorophyll and carotenoid pigments in leaves among species or at different seasons, while different slopes in PRI-albedo relationships suggest variation in the strength of the xanthophyll cycle response to variation in irradiance with more negative slopes indicating stronger xanthophyll cycle response (Gamon et al., 2023). These interpretations are consistent with the leaf-level results from this study, which showed that senescing leaves exhibited lower intercepts and shallower slopes of PRI light responses compared to green leaves (Figure S2). The decreasing intercepts in the PRI-albedo relationships of deciduous species from September to October (Figs. 4 & 5) indicate decreased chlorophyll:carotenoid pigment ratios with senescence, because deciduous species maintain their carotenoids longer as chlorophyll diminishes towards the end of the growing season (Figure S4 in the supplemental materials). This was particularly evident for the *Fraxinus* sp. that experienced an earlier leaf senescence than the other deciduous trees studied here. Changes in the slopes and intercepts in the PRI-albedo relationship from August to September likely resulted from a combination of changing pigment pool size change (more negative intercept in September than August) and changing activity of the xanthophyll cycle pigments (altered slopes). We note that these interpretations are largely based on analogous light responses between leaf- and canopy-scale, and additional work would be needed to fully confirm these interpretations, as further discussed below.

Unlike deciduous species that began leaf senescence by October, evergreen species exhibited less change in the intercepts in PRI-albedo relationships from September to October (Figs. 4 & 5), which is presumably due to the smaller adjustments in pigment concentrations occurring in evergreen foliage during this period (Magney et al., 2016; Wong et al., 2020), especially from September to October at this location (average monthly temperature is 19 °C and 12 °C in September and October, respectively). Such subtle pigment changes can be tied to important seasonal photoprotective responses as evergreen plants transition from higher photosynthetic activity during the summer growing season, to lower photosynthetic activity as colder fall temperatures emerge (Gamon et al., 2016; Wong and Gamon, 2015), and this interpretation is consistent with the general fall declines in SIF slopes in the evergreens.

Although direct assessment of photosynthetic responses was beyond the scope of this study, the changes in PRI and SIF have implications for evaluating photosynthesis in terms of the light use efficiency model. The variation in slope in the SIF-albedo relationship likely indicates a change in light use efficiency, and is particularly evident in October when fall

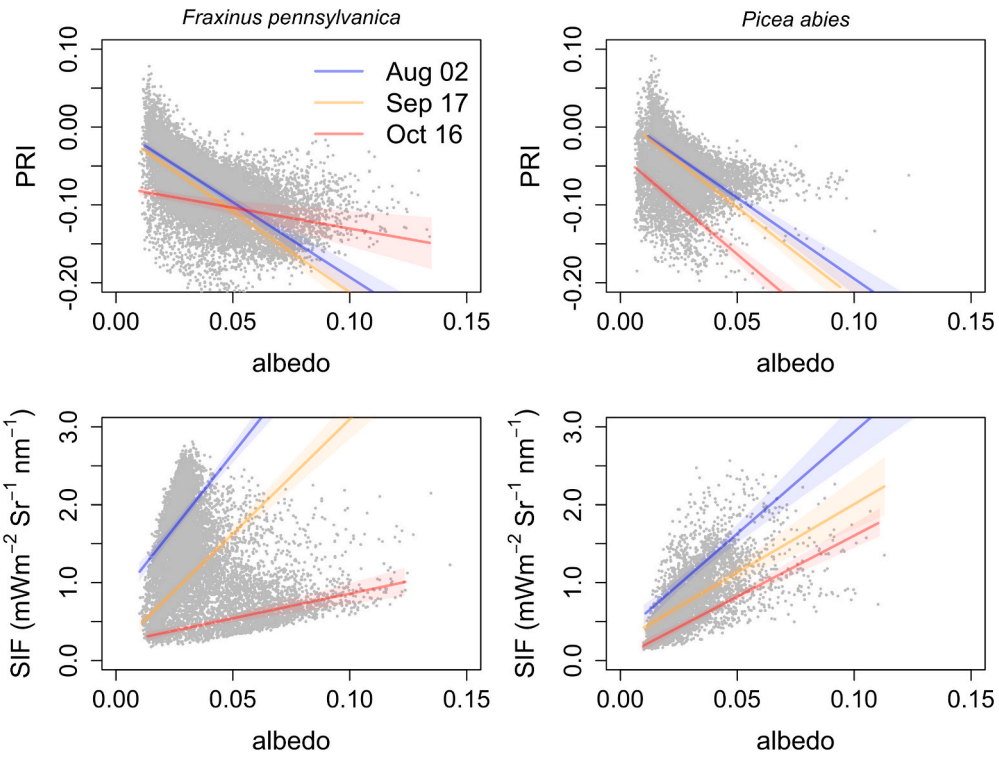

Fig. 7. PRI and SIF light responses reveal difference in photosynthetic phenology between deciduous (*Fraxinus pennsylvanica*) and evergreen species (*Picea abies*). Gray dots represent individual pixels and lines indicate the best fit lines at each sampling date. 95% confidence ribbons were estimated based on the fixed effects only (excluding tree crown-level variation within species).

senescence had begun (Figs. 4 & 5). During autumn leaf senescence, the decrease in the maximum quantum yield of photochemistry can be caused by apparent photoinhibition, which can actually be due to photoprotective responses, particularly when strong light is combined with low temperature (Porcar-Castell et al., 2014). Our results showed that while SIF values decreased from August to September (Fig. 3), the slopes in the SIF-albedo relationship did not change much for most species (Fig. 5), suggesting little change in light use efficiency from August to September.

It is worth noting that the decline in the slope of the SIF light response could also be confounded by chlorophyll losses and other pigment changes (e.g., increased anthocyanin concentration for some species) in the fall. Because of such pigment changes during the onset of leaf senescence, the PAR albedo used in the light response model may not be a fully consistent or accurate estimate of absorbed PAR (APAR), and this may complicate our interpretation of the seasonal changes in SIF light responses. These pigment changes are evident in the reflectance spectra (Figure S3) and chlorophyll index (Figure S4) and are particularly pronounced for *Fraxinus* sp. (ash). Thus, the decreasing slope in SIF-albedo between September and October for deciduous species presumably indicated a combination of decreasing chlorophyll pigments (Figure S4 in the supplemental materials) and decreasing light use efficiency due to autumn leaf senescence that is sensitive to temperature in low altitude areas (Gill et al., 2015), because the first freeze date occurred on October 14 (data obtained from the National Weather Service for Lincoln, Nebraska). Gradual declines in SIF slopes and PRI slopes for most evergreen species (Fig. 5) are likely due to the gradual transition to a sustained winter photoprotective state of evergreen plants, which also involves gradual pigment pool size changes (Springer et al., 2017, Yang et al., 2022).

Unlike PRI, we did not expect large changes in the intercept of the SIF light response, which by definition should be close to zero. The slightly non-zero intercept in SIF-albedo may be due to the fact that albedo never reached zero in the data, leading to errors in the intercepts when applying a linear extrapolation. It may also indicate slight artifacts in SIF calculation or the hierarchical modeling or could indicate additional SIF signal present in radiation contributed from surrounding pixels in these uneven tree canopies. SIF values are very sensitive to the instrument and retrieval method used, and accurate SIF readings are generally difficult to obtain (Sun et al., 2023b; Wang et al., 2022). Although the quantum yield of photochemistry cannot be directly resolved from SIF (Porcar-Castell et al., 2014), the slope in the SIF-albedo relationship can provide a way to estimate relative LUE at the canopy scale, and clear declines were seen in LUE for deciduous species, particularly for *Fraxinus* sp. which underwent early senescence.

4.2. PRI and SIF light responses among species and functional types

The photosynthetic and photoprotective responses of plants to light differ among species and environmental conditions (Bjorkman and Demmig-Adams, 1994; Demmig-Adams and Adams, 2006; Demmig-Adams et al., 2008). In our results, both PRI and SIF clearly responded to light intensity, but these light responses varied among species and functional types during the fall senescence (Figs. 4–6 and Table 2). The PRI light responses are similar to those recently reported for a deciduous forest, where differences in the PRI light responses were evident among species and for trees of different topographic positions (Gamon et al., 2023).

Evergreen and deciduous species have different photosynthetic properties associated with leaf longevity. Longer-lived evergreen leaves generally have lower photosynthetic rates but a longer period of photosynthesis and higher levels of photoprotection than shorter-lived leaves of deciduous species (Gamon et al., 1997; Wright et al., 2004; Zarter et al., 2006; Wyka et al., 2012). In August and September, deciduous species exhibited larger SIF values and steeper slopes in SIF-albedo relationships than evergreen species (Figs. 3 & 5), suggesting higher photosynthesis rate and light use efficiency for deciduous species leaves (Demmig-Adams et al., 2008; Wyka et al., 2012). In October, the

larger SIF values and steeper slope in SIF-albedo in evergreen species than deciduous species (Fig. 5) presumably reflected the maintenance of photosynthetic rate and light use efficiency longer into the fall for evergreens because evergreen leaves potentially have mechanisms that allow their leaves to conduct photosynthesis over a longer period than deciduous leaves (Demmig-Adams et al., 2008). These mechanisms include seasonal adjustment of pigment pool sizes (Demmig-Adams and Adams, 1996; Verhoeven, 2014; Bowling et al., 2018) allowing leaves to enter a protracted photoprotective state while maintaining leaf pigments instead of undergoing leaf senescence. Relative to deciduous trees, evergreen species also exhibited relatively small seasonal changes in slope and intercept in the PRI-albedo relationship (Figs. 2, 4 & 7). This suggests a more stable seasonal pattern of photosynthesis as is expected from evergreen leaves having a longer leaf life-span associated with lower responsiveness of leaf traits to changes in environmental factors (Wyka et al., 2012).

A within-canopy heterogeneous light environment, caused by self-shading or shading by neighboring trees, can affect leaf structural and physiological traits in both deciduous and evergreen species (Bjorkman and Demmig-Adams, 1994; Yoshimura, 2010). The strength of structural and functional plasticity of leaves in response to the crown light gradient is presumably species specific and varies over time. In this study, the interspecific PRI and SIF light responses were larger in October than in August and September (Figs. 5–7), revealing enhanced functional differences during fall senescence. It is interesting that minimal interspecific differences in PRI and SIF light responses emerged in the September data (Fig. 6), which also had minimal among-species spectral variation and lowest species classification accuracy from imaging spectrometry (data not shown). These contrasting seasonal responses suggest seasonal patterns of SIF and PRI could enhance our ability to detect functional differences between species and vegetation types, which may be enhanced during periods or conditions of senescence.

Fraxinus pennsylvanica exhibited clearly different slope and intercept in PRI response and slope in SIF response from other species in September (Figs. 6 & 7), which is likely due to an early senescence of this species whose leaf color change can begin in the first week of September. This early senescence was easily recognizable from the PRI and SIF light responses, but not from canopy average PRI and SIF values (c.f. Figs. 3 & 5), demonstrating a clear benefit of analyzing PRI and SIF as light responses to reveal species' functional differences in seasonal patterns of photoregulation and photoprotection. In Nebraska, this species has been in decline due to the spread of the emerald ash borer (*Agrilus planipennis*), an introduced species, and it is likely that these measurements detected this decline as a rapid fall senescence. These trees were subsequently removed by campus grounds crew between 2021 and 2023. This intriguing pattern for ash indicates that PRI and SIF light responses might serve as early indicators of tree decline. Similar work has shown that fluorescence and PRI can contribute to early detection of olive tree decline prior to detection by visible or molecular methods (Zarco-Tejada et al., 2018) and reflectance indices can detect early symptoms of oak decline (Sapes et al., 2022).

4.3. Caveats and future directions

In this study, we introduce a light response framework for analyzing airborne PRI and SIF values by accounting for illumination as albedo, directly derived from imagery. This approach successfully differentiated photosynthetic properties among tree crowns, species, and functional types across seasons. However, we note that more work is needed to test this light response framework to further validate our interpretations and provide a more complete understanding of the mechanisms involved.

At the canopy level, both PRI and SIF (e.g., Barton and North, 2001; Biriukova et al., 2020; Chang et al., 2021) can be confounded by the sun-view geometry varying at both diurnal and seasonal temporal scales. In this work, we limited this angular effect by collecting data close to solar noon and using lens with relatively narrow field of view (the FOV of Kestrel and Ibis are 40° and 32.3°, respectively). Due to practical reasons (e.g., cost, weather suitability and personnel availability), acquiring intensive flight lines with multiple sun-view angles is challenging. A more careful multi-angular study using ground-based observations (e.g., Biriukova et al., 2020; Bai et al., 2023) could be used to characterize the angular effects on the parameters (e.g., slope and intercept) of the PRI- and SIF-light responses. In addition, our results were obtained between mid-season and autumn senescence. A more completed seasonal data, including green-up and senescence, could give us the full picture of the PRI- and SIF-light responses through the season.

A large number of alternative expressions have been proposed to delineate the physiological and structure effects on SIF (e.g., Yang et al., 2020; Zeng et al., 2021 and PRI (e.g., Van Wittenberghe et al., 2021; Woodgate et al., 2019). Many of these indices have been developed for relatively homogeneous fields (e.g., crops) or targeted at certain species using leaf level measurements, so may not be applicable in this complex urban forest setting. The escape probability correction has been proposed to account for the structural influence of canopies on the measured SIF. Theoretically, SIF escape from the canopy can be estimated with SIF radiative transfer models depicting specified 3D structure of plant canopy. However, this correction is often hampered by the high computation demand and various assumptions and limitation in the SIF escape rate formulations (Sun et al., 2023a, 2023b), which become particularly challenging in structurally complex forests so was not attempted in our study. The light response approach proposed here relies on a per-pixel based calculation rather than temporally or spatially averaged values, making the SIF escape rate correction (e.g., using FCVI or NIRv) a challenge due to the difficulties in deriving the accurate pixelwise "true" reflectance within tree crown.

Modified PRI indices have been developed to delineate the short term ("facultative") and long-term ("constitutive") effects. For example, by accounting for the constitutive effects, triPRI (Woodgate et al., 2019) was designed to be sensitive to facultative effects when developed using leaf level measurements from mature eucalyptus forests. Our results are generally consistent with these conclusions, and suggest that canopy light responses from airborne imaging spectrometry work in a similar way to leaf responses when applied to multiple species' crowns across seasons (Figures S5 and S6 in the supplemental materials). The triPRI reduced the intercept differences and reversed the slope patterns seen in the PRI light response (Figs. 5 and S6 in the supplemental materials), indicating a more positive slope with xanthophyll cycle de-epoxidation (Woodgate et al., 2019), a pattern consistent with the results shown here. Despite these encouraging results, an explicit test of the various different versions of PRI and SIF reported in the literature was beyond the scope of this study, which focused on using airborne imaging spectrometry to detect functional differences in photosynthetic and photoprotective properties between species and functional groups across seasons. By using the 'raw' PRI, SIF, and albedo values directly derived from the airborne data to capture variation in structure and physiology, we demonstrate the potential of this light response approach with the caveat that further work would be needed to further validate and optimize these methods.

While PRI and SIF are known to be physiologically related, definitive interpretations of their light-dependent variation are still uncertain. Here, we took the first steps towards defining these interpretations by documenting patterns of interspecific, intraspecific, and seasonal variation. However, much remains to be learned in terms of mooring these remote sensing derived parameters to clear physiological meanings. Due to the non-homogenous forest structure (Fig. 1) and lack of explicit 3-D structural data, a full exploration of the physiological and structural differences among leaves within tree crown would likely not be tractable in this setting, but would be a valuable future direction. We would expect that combining a set of explicit leaf level measurements, likely including sampling of pigments, irradiance, and photosynthesis as well as leaf optical properties, fine scale structure information derived from LiDAR or structure from motion (SfM) data, specified taxonomic,

functional, and physiological information collected on the ground using tree inventory plots (e.g., Regaieg et al., 2021; Gamon et al., 2023) and modeling approaches (e.g., the Discrete Anisotropic Radiative Transfer (DART) model; Gastellu-Etchegorry et al., 2004) to describe the detailed within canopy light environment could be further used to evaluate PRI and SIF (along with other indices) in this light response framework.

5. Conclusions

Unlike commonly measured plant traits like leaf mass per area, the photosynthetic and photoprotective behavior revealed through optical properties related to the functioning of pigments is dynamic in space and time and critical to understanding plant responses to variable environmental conditions. This dynamism is captured by parameters quantifying variation in PRI and SIF with respect to light intensity, revealing additional information beyond PRI and SIF canopy-average values, which often obscure the light-dependent responses of individuals and species. Similar to plant trait analysis, the synergistic analysis of PRI and SIF with illumination provides key information about the functional differences among individual trees, species, functional types and reveals seasonal effects on these differences. Our novel approach to treating PRI and SIF light response parameters as dynamic functional traits has broad implications for detecting forest photosynthetic activity and monitoring forest stress in variable environments and assessing functional diversity across species and individuals using airborne remote sensing.

CRediT authorship contribution statement

Ran Wang: Writing – review & editing, Writing – original draft, Methodology, Funding acquisition, Formal analysis, Data curation, Conceptualization. **John A. Gamon:** Writing – review & editing, Resources, Methodology, Funding acquisition, Conceptualization. **Sabrina E. Russo:** Writing – review & editing, Methodology, Conceptualization. **Aime Valentin Nishimwe:** Writing – review & editing, Formal analysis. **Hugh Ellerman:** Writing – review & editing, Formal analysis. **Brian Wardlow:** Writing – review & editing, Project administration, Funding acquisition, Data curation.

Declaration of competing interest

The authors declare that they have no known competing financial interests or personal relationships that could have appeared to influence the work reported in this paper.

Data availability

Data will be made available on request.

Acknowledgements

We thank Rick Perk for acquiring the airborne data and Jeff Culbertson and Rama Cheruku from Landscape Services at UNL for providing the campus tree inventory data. We appreciate help from Dr. Sergio Cogliati in implementing SIF retrieval method. This work was supported by the European Space Agency (ESA) “PhotoProxy” contract via Forschungszentrum Jülich (ESA Contract no. 4000125731/19/NL/LF), United States Department of Agriculture McIntire-Stennis award (7002574) and UNL startup funding to JAG, a Nebraska View grant (25-6238-0884-004) to BW, and a NASA Nebraska Space Grant (44-0307-1026-335) to RW.

Appendix A. Supplementary data

Supplementary data to this article can be found online at https://doi.org/10.1016/j.rse.2024.114295.

References

Adams III, W.W., Demmig-Adams, B., Rosenstiel, T.N., Brightwell, A.K., Ebbert, V., 2002. The employment of zeaxanthin-dependent photoprotective. Plant Biol. 4, 545–557.
Badgley, G., Field, C.B., Berry, J.A., 2017. Canopy near-infrared reflectance and terrestrial photosynthesis. Sci. Adv. 3, e1602244 https://doi.org/10.1126/sciadv.1602244.
Bai, G., Ge, Y., Leavitt, B., Gamon, J.A., Scoby, D., 2023. Goniometer in the air: Enabling BRDF measurement of crop canopies using a cable-suspended plant phenotyping platform. Biosyst. Eng. 230, 344–360.
Barton, K., 2009. MUMIN: Multi-modelinference. R Package v.0.12.0 [WWW document] URL. https://r-forge.r-project.org/projects/mumin/. accessed 23 April 2021.
Barton, C.V.M., North, P.R.J., 2001. Remote sensing of canopy light use efficiency using the photochemical reflectance index model and sensitivity analysis. Remote Sens. Environ. 78 (3), 264–273. https://doi.org/10.1016/S0034-4257(01)00224-3.
Bates, D., Machler, M., Bolker, B.M., Walker, S.C., 2015. Fitting linear mixed-effects models using LME4. J. Stat. Software 67, 1–48.
Benjamini, Y., Hochberg, Y., 1995. Controlling the false discovery rate : A practical and powerful approach to multiple testing. J. R. Stat. Soc. 57, 289–300.
Berk, A., Anderson, G.P., Acharya, P.K., Shettle, E.P., 2008. MODTRAN5. 2.0. 0 User’s Manual. Spectr. Sci. Inc., Burlingt. MA, Air Force Res. Lab., Hanscom MA.
Biriukova, K., Celesti, M., Evdokimov, A., Pacheco-Labrador, J., Julitta, T., Migliavacca, M., Giardino, C., Miglietta, F., Colombo, R., Panigada, C., Rossini, M., 2020. Effects of varying solar-view geometry and canopy structure on solar-induced chlorophyll fluorescence and PRI. Int. J. Appl. Earth Obs. Geoinf. 89 (January), 102069 https://doi.org/10.1016/j.jag.2020.102069.
Bjorkman, O., Demmig-Adams, B., 1994. Regulation of photosynthetic light energy capture, conversion, and dissipation in leaves of higher plants. In: Ecolphysiology of Photosynthesis. Springer, pp. 17–47.
Bowling, D.R., Logan, B.A., Hufkens, K., Aubrecht, D.M., Richardson, A.D., Burns, S.P., Anderegg, W.R.L., Blanken, P.D., Eiriksson, D.P., 2018. Limitations to winter and spring photosynthesis of a Rocky Mountain subalpine forest. Agric. For. Meteorol. 252, 241–255. https://doi.org/10.1016/j.agrformet.2018.01.025.
Carrère, V., Conel, J.E., 1993. Recovery of atmospheric water vapor total column abundance from imaging spectrometer data around 940 nm - sensitivity analysis and application to Airborne Visible/Infrared Imaging Spectrometer (AVIRIS) data. Remote Sens. Environ. 44 (2–3), 179–204. https://doi.org/10.1016/0034-4257(93)90015-P.
Chang, C.Y., Zhou, R., Kira, O., Marri, S., Skovira, J., Gu, L., Sun, Y., 2020. An Unmanned Aerial System (UAS) for concurrent measurements of solar-induced chlorophyll fluorescence and hyperspectral reflectance toward improving crop monitoring. Agric. For. Meteorol. 294, 108145 https://doi.org/10.1016/j.agrformet.2020.108145.
Chang, C.Y., Wen, J., Han, J., Kira, O., LeVonne, J., Melkonian, J., Riha, S.J., Skovira, J., Ng, S., Gu, L., Wood, J.D., Näthe, P., Sun, Y., 2021. Unpacking the drivers of diurnal dynamics of sun-induced chlorophyll fluorescence (SIF): Canopy structure, plant physiology, instrument configuration and retrieval methods. Remote Sens. Environ. 265 https://doi.org/10.1016/j.rse.2021.112672.
Cogliati, S., Verhoef, W., Kraft, S., Sabater, N., Alonso, L., Vicent, J., Moreno, J., Drusch, M., Colombo, R., 2015. Retrieval of sun-induced fluorescence using advanced spectral fitting methods. Remote Sens. Environ. 169, 344–357. https://doi.org/10.1016/j.rse.2015.08.022.
Damm, A., Cogliati, S., Colombo, R., Fritsche, L., Genangeli, A., Genesio, L., Hanus, J., Peressotti, A., Rademske, P., Rascher, U., Schuettemeyer, D., Siegmann, B., Sturm, J., Miglietta, F., 2022. Response times of remote sensing measured sun-induced chlorophyll fluorescence, surface temperature and vegetation indices to evolving soil water limitation in a crop canopy. Remote Sens. Environ. 273, 112957 https://doi.org/10.1016/j.rse.2022.112957.
Dechant, B., Ryu, Y., Badgley, G., Zeng, Y., Berry, J.A., Zhang, Y., Goulas, Y., Li, Z., Zhang, Q., Kang, M., Li, J., Moya, I., 2020. Canopy structure explains the relationship between photosynthesis and sun-induced chlorophyll fluorescence in crops. Remote Sens. Environ. 241 https://doi.org/10.1016/j.rse.2020.111733.
Demmig-Adams, B., Adams, W.W., 1996. The role of xanthophyll cycle carotenoids in the protection of photosynthesis. Trends Plant Sci. 1, 21–26. https://doi.org/10.1016/S1360-1385(96)80019-7.
Demmig-Adams, B., Adams, W.W., 2006. Photoprotection in an ecological context: The remarkable complexity of thermal energy dissipation. New Phytol. 172, 11–21. https://doi.org/10.1111/j.1469-8137.2006.01835.x.
Demmig-Adams, B., Adams, W.W., Barker, D.H., Logan, B.A., Bowling, D.R., Verhoeven, A.S., 1996. Using chlorophyll fluorescence to assess the fraction of absorbed light allocated to thermal dissipation of excess excitation. Physiol. Plant. 98, 253–264.
Demmig-Adams, B., Adams III, W.W., Mattoo, A.K. (Eds.), 2008. Photoprotection, Photoinhibition, Gene Regulation and Environment. Springer, Dordrecht.
Drusch, M., Moreno, J., Del Bello, U., Franco, R., Goulas, Y., Huth, A., Kraft, S., Middleton, E.M., Miglietta, F., Mohammed, G., Nedbal, L., Rascher, U., Schüttemeyer, D., Verhoef, W., 2017. The FLuorescence Explorer mission concept — ESA ’ s Earth explorer 8. IEEE Trans. Geosci. Remote Sens. 55, 1273–1284.
Gamon, J.A., Berry, J.A., 2012. Facultative and constitutive pigment effects on the Photochemical Reflectance Index (PRI) in sun and shade conifer needles. Isr. J. Plant Sci. 60, 85–95. https://doi.org/10.1560/IJPS.60.1-2.85.
Gamon, J.A., Qiu, H.-L., 1999. Ecological applications of remote sensing at multiple scales. In: Pugnaire, F.I., Valladares, F. (Eds.), Handbook of Functional Plant Ecology. Marcel Dekker, Inc., New York, pp. 805–846.
Gamon, J.A., Surfus, J.S., 1999. Accessing leaf pigment content and activity with a reflectometer. New Phytol. 143, 105–117.

Gamon, J.A., Field, C.B., Goulden, M.L., Griffin, K.L., Hartley, A.E., Joel, G., Penuelas, J., Valentini, R., 1995. Relationships between NDVI, canopy structure, and photosynthesis in three californian vegetation types. Ecol. Appl. 5, 28–41.
Gamon, J.A., Serrano, L., Surfus, S., 1997. The photochemical reflectance index : an optical indicator of photosynthetic radiation use efficiency across species, functional types, and nutrient levels. Oecologia 112, 492–501.
Gamon, J.A., Kitajima, K., Mulkey, S.S., Serrano, L., Wright, S.J., 2005. Diverse optical and photosynthetic properties in a neotropical dry forest during the dry season: Implications for remote estimation of photosynthesis. Biotropica 37, 547–560.
Gamon, J.A., Huemmrich, K.F., Wong, C.Y.S., Ensminger, I., Garrity, S., Hollinger, D.Y., Noormets, A., Peñuelas, J., 2016. A remotely sensed pigment index reveals photosynthetic phenology in evergreen conifers. Proc. Natl. Acad. Sci. USA 113, 13087–13092. https://doi.org/10.1073/pnas.1606162113.
Gamon, J.A., Wang, R., Russo, S.E., 2023. Contrasting photoprotective responses of forest trees revealed using PRI light responses sampled with airborne imaging spectrometry. New Phytol. https://doi.org/10.1111/nph.18754.
Garbulsky, M.F., Peñuelas, J., Papale, D., Ardö, J., Goulden, M.L., Kiely, G., Richardson, A.D., Rotenberg, E., Veenendaal, E.M., Filella, I., 2010. Patterns and controls of the variability of radiation use efficiency and primary productivity across terrestrial ecosystems. Glob. Ecol. Biogeogr. 19, 253–267. https://doi.org/10.1111/j.1466-8238.2009.00504.x.
Garbulsky, M.F., Peñuelas, J., Gamon, J.A., Inoue, Y., Filella, I., 2011. The photochemical reflectance index (PRI) and the remote sensing of leaf, canopy and ecosystem radiation use efficiencies: A review and meta-analysis. Remote Sens. Environ. 115, 281–297. https://doi.org/10.1016/j.rse.2010.08.023.
Gastellu-Etchegorry, J.P., Martin, E., Gascon, F., 2004. Dart: a 3d model for simulating satellite images and studying surface radiation budget. Int. J. Remote Sens. 250 (1), 73–96.
Gill, A.L., Gallinat, A.S., Sanders-DeMott, R., Rigden, A.J., Short Gianotti, D.J., Mantooth, J.A., Templer, P.H., 2015. Changes in autumn senescence in northern hemisphere deciduous trees: A meta-analysis of autumn phenology studies. Ann. Bot. 116, 875–888. https://doi.org/10.1093/aob/mcv055.
Hmimina, G., Dufrêne, E., Soudani, K., 2014. Relationship between photochemical reflectance index and leaf ecophysiological and biochemical parameters under two different water statuses: Towards a rapid and efficient correction method using real-time measurements. Plant Cell Environ. 37, 473–487. https://doi.org/10.1111/pce.12171.
Huete, A., Didan, K., Miura, T., Rodriguez, E.P., Gao, X., Ferreira, L.G., 2002. Overview of the radiometric and biophysical performance of the MODIS vegetation indices. Remote Sens. Environ. 83, 195–213. https://doi.org/10.1016/S0034-4257(02)00096-2.
Jahns, P., Holzwarth, A.R., 2012. The role of the xanthophyll cycle and of lutein in photoprotection of photosystem II. Biochim. Biophys. Acta Bioenerg. 1817, 182–193. https://doi.org/10.1016/j.bbabio.2011.04.012.
Kaufman, Y.J., Tanre, D., Remer, L.A., Vermote, E.F., Chu, A., Holben, B.N., 1997. Operational remote sensing of tropospheric aerosol over land from EOS moderate resolution imaging spectroradiometer. J. Geophys. Res. Atmos. 102 (14), 17051–17067. https://doi.org/10.1029/96jd03988.
Liu, Y.K., Li, C.R., Ma, L.L., Qian, Y.G., Wang, N., Gao, C.X., Tang, L.L., 2019. Land surface reflectance retrieval from optical hyperspectral data collected with an unmanned aerial vehicle platform. Opt. Express 27 (5), 7174. https://doi.org/10.1364/oe.27.007174.
Lüdecke, D., 2018. GGEFFECTS: tidy data frames ofmarginal effects from regression models. J. Open Source Software 3, 772.
Magney, T.S., Vierling, L.A., Eitel, J.U.H., Huggins, D.R., Garrity, S.R., 2016. Response of high frequency Photochemical Reflectance Index (PRI) measurements to environmental conditions in wheat. Remote Sens. Environ. 173, 84–97. https://doi.org/10.1016/j.rse.2015.11.013.
Magney, T.S., Bowling, D.R., Logan, B.A., Grossmann, K., Stutz, J., Blanken, P.D., Burns, S.P., Cheng, R., Garcia, M.A., Köhler, P., Lopez, S., Parazoo, N.C., Raczka, B., Schimel, D., Frankenberg, C., 2019. Mechanistic evidence for tracking the seasonality of photosynthesis with solar-induced fluorescence. Proc. Natl. Acad. Sci. 201900278 https://doi.org/10.1073/pnas.1900278116.
Magney, T.S., Barnes, M.L., Yang, X., 2020. On the covariation of chlorophyll fluorescence and photosynthesis across scales. Geophys. Res. Lett. 47, 1–12. https://doi.org/10.1029/2020GL091098.
Marrs, J.K., Reblin, J.S., Logan, B.A., Allen, D.W., Reinmann, A.B., Bombard, D.M., Tabachnik, D., Hutyra, L.R., 2020. Solar-induced fluorescence does not track photosynthetic carbon assimilation following induced stomatal closure. Geophys. Res. Lett. 47, 1–11. https://doi.org/10.1029/2020GL087956.
McGill, R., Tukey, J.W., Larsen, W.A., 1978. Variations of box plots. Am. Stat. 32 (1), 12–16.
Mohammed, G.H., Colombo, R., Middleton, E.M., Rascher, U., van der Tol, C., Nedbal, L., Goulas, Y., Pérez-Priego, O., Damm, A., Meroni, M., Joiner, J., Cogliati, S., Verhoef, W., Malenovský, Z., Gastellu-Etchegorry, J.P., Miller, J.R., Guanter, L., Moreno, J., Moya, I., Berry, J.A., Frankenberg, C., Zarco-Tejada, P.J., 2019. Remote sensing of solar-induced chlorophyll fluorescence (SIF) in vegetation: 50 years of progress. Remote Sens. Environ. 231, 111177 https://doi.org/10.1016/j.rse.2019.04.030.
Monteith, J.L., 1972. Solar radition and productivity in tropical ecosystems. J. Appl. Ecol. https://doi.org/10.2307/2401901.
Monteith, J.L., 1977. Climate and the efficiency of crop production in Britain. Philos. T. Roy. Soc. B 281, 277–294. https://doi.org/10.1098/rstb.1977.0140.
Nakagawa, S., Schielzeth, H., 2013. A general and simple method for obtaining R2 from generalized linear mixed-effects models. Methods Ecol. Evol. 4, 133–142. https://doi.org/10.1111/j.2041-210x.2012.00261.x.
Niyogi, K.K., Björkman, O., Grossman, A.R., 1997. The roles of specific xanthophylls in photoprotection. Proc. Natl. Acad. Sci. USA 94, 14162–14167. https://doi.org/10.1073/pnas.94.25.14162.
Öquist, G., Huner, N.P.A., 2003. Photosynthesis of overwintering evergreen plants. Annu. Rev. Plant Biol. 54, 329–355. https://doi.org/10.1146/annurev.arplant.54.072402.115741.
Paul-Limoges, E., Damm, A., Hueni, A., Liebisch, F., Eugster, W., Schaepman, M.E., Buchmann, N., 2018. Effect of environmental conditions on sun-induced fluorescence in a mixed forest and a cropland. Remote Sens. Environ. 219, 310–323. https://doi.org/10.1016/j.rse.2018.10.018.
Porcar-Castell, A., Tyystjärvi, E., Atherton, J., Van Der Tol, C., Flexas, J., Pfündel, E.E., Moreno, J., Frankenberg, C., Berry, J.A., 2014. Linking chlorophyll a fluorescence to photosynthesis for remote sensing applications: Mechanisms and challenges. J. Exp. Bot. 65, 4065–4095. https://doi.org/10.1093/jxb/eru191.
R Core Development Team, 2019. A language andenvironmentfor statistical computing (v.3.6.2). R Foundation for Statistical Computing, Vienna, Austria.
Regaieg, O., et al., 2021. Assessing impacts of canopy 3D structure on chlorophyll fluorescence radiance and radiative budget of deciduous forest stands using DART. Remote Sens. Environ. 265, 112673.
Running, S.W., Nemani, R.R., Heinsch, F.A., Zhao, M., Reeves, M., Hashimoto, H., 2004. A continuous satellite-derived measure of global terrestrial primary production. BioScience 54 (6), 547–560.
Sapes, G., Lapadat, C., Schweiger, A.K., Juzwik, J., Montgomery, R., Gholizadeh, H., Townsend, P.A., Gamon, J.A., Cavender-Bares, J., 2022. Canopy spectral reflectance detects oak wilt at the landscape scale using phylogenetic discrimination. Remote Sens. Environ. 273, 112961 https://doi.org/10.1016/j.rse.2022.112961.
Shekhar, A., Buchmann, N., Gharun, M., 2022. How well do recently reconstructed solar-induced fluorescence datasets model gross primary productivity? Remote Sens. Environ. 283, 113282 https://doi.org/10.1016/j.rse.2022.113282.
Smith, W.K., Biederman, J.A., Scott, R.L., Moore, D.J.P., He, M., Kimball, J.S., Yan, D., Hudson, A., Barnes, M.L., MacBean, N., Fox, A.M., Litvak, M.E., 2018. Chlorophyll fluorescence better captures seasonal and interannual gross primary productivity dynamics across dryland ecosystems of Southwestern North America. Geophys. Res. Lett. 45, 748–757. https://doi.org/10.1002/2017GL075922.
Springer, K.R., Wang, R., Gamon, J.A., 2017. Parallel seasonal patterns of photosynthesis, fluorescence, and reflectance indices in boreal trees. Remote Sens. 9 (7), 1–18.
Sun, Y., Gu, L., Wen, J., van der Tol, C., Porcar-Castell, A., Joiner, J., Chang, C.Y., Magney, T., Wang, L., Hu, L., Rascher, U., Zarco-Tejada, P., Barrett, C.B., Lai, J., Han, J., Luo, Z., 2023a. From remotely sensed solar-induced chlorophyll fluorescence to ecosystem structure, function, and service: Part I—Harnessing theory. Glob. Chang. Biol. 29, 2926–2952. https://doi.org/10.1111/gcb.16634.
Sun, Y., Wen, J., Gu, L., Joiner, J., Chang, C.Y., van der Tol, C., Porcar- Castell, A., Magney, T., Wang, L., Hu, L., Rascher, U., Zarco-Tejada, P., Barrett, C.B., Lai, J., Han, J., Luo, Z., 2023b. From remotely- sensed SIF to ecosystem structure, function, and service: Part II— Harnessing data. Glob. Chang. Biol. https://doi.org/10.1111/gcb.16646.
Tagliabue, G., Panigada, C., Dechant, B., Baret, F., Cogliati, S., Colombo, R., Migliavacca, M., Rademske, P., Schickling, A., Schüttemeyer, D., Verrelst, J., Rascher, U., Ryu, Y., Rossini, M., 2019. Exploring the spatial relationship between airborne-derived red and far-red sun-induced fluorescence and process-based GPP estimates in a forest ecosystem. Remote Sens. Environ. 231, 111272 https://doi.org/10.1016/j.rse.2019.111272.
USDA, 2018. Farm Service Agency National Agriculture Imagery Program (NAIP) Digital Ortho Photo Imagery [WWW document] URL. https://www.usgs.gov/centers/eros/science/usgs-eros-archive-aerial-photography-national-agriculture-imagery-program-naip.
Van Wittenberghe, S., Laparra, V., García-Plazaola, J.I., Fernández-Marín, B., Porcar-Castell, A., Moreno, J., 2021. Combined dynamics of the 500–600 nm leaf absorption and chlorophyll fluorescence changes in vivo: Evidence for the multifunctional energy quenching role of xanthophylls. Biochimica et Biophysica Acta (BBA)-Bioenergetics 1862 (2), 148351.
Verhoef, W., Bach, H., 2003. Simulation of hyperspectral and directional radiance images using coupled biophysical and atmospheric radiative transfer models. *Remote Sens. Environ.* 87 (1), 23–41. https://doi.org/10.1016/S0034-4257(03)00143-3.
Verhoeven, A., 2014. Sustained energy dissipation in winter evergreens. New Phytol. 201, 57–65. https://doi.org/10.1111/nph.12466.
Verma, M., Schimel, D., Evans, B., Frankenberg, C., Beringer, J., Drewry, D.T., Magney, T., Marang, I., Hutley, L., Moore, C., Eldering, A., 2017. Effect of environmental conditions on the relationship between solar-induced fluorescence and gross primary productivity at an OzFlux grassland site. J. Geophys. Res. Biogeosci. 122, 716–733. https://doi.org/10.1002/2016JG003580.
Wang, R., Gamon, J.A., Moore, R., Zygielbaum, A.I., Arkebauer, T.J., Perk, R., Leavitt, B., Cogliati, S., Wardlow, B., Qi, Y., 2021. Errors associated with atmospheric correction methods for airborne imaging spectroscopy: Implications for vegetation indices and plant traits. Remote Sens. Environ. 265, 112663 https://doi.org/10.1016/j.rse.2021.112663.
Wang, R., Gamon, J.A., Hmimina, G., Cogliati, S., Zygielbaum, A.I., Arkebauer, T.J., Suyker, A., 2022. Harmonizing solar induced fluorescence across spatial scales, instruments, and extraction methods using proximal and airborne remote sensing : A multi-scale study in a soybean field. Remote Sens. Environ. 281, 113268 https://doi.org/10.1016/j.rse.2022.113268.
Wieneke, S., Burkart, A., Cendrero-Mateo, M.P., Julitta, T., Rossini, M., Schickling, A., Schmidt, M., Rascher, U., 2018. Linking photosynthesis and sun-induced fluorescence at sub-daily to seasonal scales. Remote Sens. Environ. 219, 247–258. https://doi.org/10.1016/j.rse.2018.10.019.

Wong, C.Y.S., Gamon, J.A., 2015. Three causes of variation in the photochemical reflectance index (PRI) in evergreen conifers. New Phytol. 206, 187–195. https://doi.org/10.1111/nph.13159.

Wong, C.Y.S., D'Odorico, P., Arain, M.A., Ensminger, I., 2020. Tracking the phenology of photosynthesis using carotenoid-sensitive and near-infrared reflectance vegetation indices in a temperate evergreen and mixed deciduous forest. New Phytol. 226, 1682–1695. https://doi.org/10.1111/nph.16479.

Wong, C.Y.S., Mercado, L.M., Arain, M.A., Ensminger, I., 2022. Remotely sensed carotenoid dynamics improve modelling photosynthetic phenology in conifer and deciduous forests. Agric. For. Meteorol. 321 (October 2021), 108977 https://doi.org/10.1016/j.agrformet.2022.108977.

Woodgate, W., Suarez, L., van Gorsel, E., Cernusak, L.A., Dempsey, R., Devilla, R., Held, A., Hill, M.J., Norton, A.J., 2019. tri-PRI: A three band reflectance index tracking dynamic photoprotective mechanisms in a mature eucalypt forest. Agric. For. Meteorol. 272–273 (April), 187–201. https://doi.org/10.1016/j.agrformet.2019.03.020.

Wright, I.J., Reich, P.B., Westoby, M., Ackerly, D.D., Baruch, Z., Bongers, F., Cavender-Bares, J., Chapin, T., Cornelissen, J.H.C., Diemer, M., Flexas, J., Garnier, E., Groom, P.K., Gulias, J., Hikosaka, K., Lamont, B.B., Lee, T., Lee, W., Lusk, C., Midgley, J.J., Navas, M.-L., Niinemets, U., Oleksyn, J., Osada, N., Poorter, H., Poot, P., Prior, L., Pyankov, V.I., Roumet, C., Thomas, S.C., Tjoelker, M.G., Veneklaas, E.J., Villar, R., 2004. The worldwide leaf economics spectrum. Nature 428, 821–827. https://doi.org/10.1038/nature02403.

Wyka, T.P., Oleksyn, J., Żytkowiak, R., Karolewski, P., Jagodziński, A.M., Reich, P.B., 2012. Responses of leaf structure and photosynthetic properties to intra-canopy light gradients: A common garden test with four broadleaf deciduous angiosperm and seven evergreen conifer tree species. Oecologia 170, 11–24. https://doi.org/10.1007/s00442-012-2279-y.

Yang, P., van der Tol, C., Campbell, P.K.E., Middleton, E.M., 2020. Fluorescence Correction Vegetation Index (FCVI): A physically based reflectance index to separate physiological and non-physiological information in far-red sun-induced chlorophyll fluorescence. Remote Sens. Environ. 240, 111676.

Yang, J.C., Magney, T.S., Albert, L.P., Richardson, A.D., Frankenberg, C., Stutz, J., Grossmann, K., Burns, S.P., Seyednasrollah, B., Blanken, P.D., Bowling, D.R., 2022. Gross primary production (GPP) and red solar induced fluorescence (SIF) respond differently to light and seasonal environmental conditions in a subalpine conifer forest. Agric. For. Meteorol. 317, 108904 https://doi.org/10.1016/j.agrformet.2022.108904.

Yoshimura, K., 2010. Irradiance heterogeneity within crown affects photosynthetic capacity and nitrogen distribution of leaves in Cedrela sinensis. Plant Cell Environ. 33, 750–758. https://doi.org/10.1111/j.1365-3040.2009.02100.x.

Yuan, W., Liu, S., Zhou, G., Zhou, G., Tieszen, L.L., Baldocchi, D., Bernhofer, C., Gholz, H., Goldstein, A.H., Goulden, M.L., Hollinger, D.Y., Hu, Y., Law, B.E., Stoy, P.C., Vesala, T., Wofsy, S.C., 2007. Deriving a light use efficiency model from eddy covariance flux data for predicting daily gross primary production across biomes. Agric. For. Meteorol. 143, 189–207. https://doi.org/10.1016/j.agrformet.2006.12.001.

Zarco-Tejada, P.J., Camino, C., Beck, P.S.A., et al., 2018. Previsual symptoms of Xylella fastidiosainfection revealed in spectral plant-trait alterations. Nature Plants 4, 432–439. https://doi.org/10.1038/s41477-018-0189-7.

Zarter, C.R., Demmig-Adams, B., Ebbert, V., Adamska, I., Adams, W.W., 2006. Photosynthetic capacity and light harvesting efficiency during the winter-to-spring transition in subalpine conifers. New Phytol. 172, 283–292. https://doi.org/10.1111/j.1469-8137.2006.01816.x.

Zeng, Y., Badgley, G., Dechant, B., Ryu, Y., Chen, M., Berry, J.A., 2019. A practical approach for estimating the escape ratio of near-infrared solar-induced chlorophyll fluorescence. Remote Sens. Environ. 232, 111209 https://doi.org/10.1016/j.rse.2019.05.028.

Zeng, Y., Hao, D., Badgley, G., Damm, A., Rascher, U., Ryu, Y., Johnson, J., Krieger, V., Wu, S., Qiu, H., Liu, Y., Berry, J., Chen, M., et al., 2021. Estimating near-infrared reflectance of vegetation from hyperspectral data. Remote Sensing of Environment 267.

Zeng, Y., Hao, D., Huete, A., Dechant, B., Berry, J., Chen, J.M., Joiner, J., Frankenberg, C., Bond-Lamberty, B., Ryu, Y., Xiao, J., Asrar, G.R., Chen, M., 2022. Optical vegetation indices for monitoring terrestrial ecosystems globally. Nat. Rev. Earth Environ. 3, 477–493. https://doi.org/10.1038/s43017-022-00298-5.

Zhang, Y., Fang, J., Smith, W.K., Wang, X., Gentine, P., Scott, R., Migliavacca, M., Jeong, S., Litvak, M., Piao, S., Zhou, S., 2023. Satellite solar-induced chlorophyll fluorescence tracks physiological drought stress development during 2020 southwest US drought. Glob. Chang. Biol. 29, 3395–3408.